Biochimica et Biophysica Acta 1813 (2011) 1906–1916

Contents lists available at ScienceDirect

Biochimica et Biophysica Acta

journal homepage: www.elsevier.com/locate/bbamcr

Extracellular loops 1 and 3 and their associated transmembrane regions of the calcitonin receptor-like receptor are needed for CGRP receptor function

James Barwell [a], Alex Conner [b], David R. Poyner [a,*]

[a] School of Life and Health Sciences, Aston University, Birmingham, B4 7ET, UK
[b] Warwick Medical School, University of Warwick, Coventry, CV4 7AL, UK

ARTICLE INFO

Article history:
Received 21 April 2011
Received in revised form 31 May 2011
Accepted 8 June 2011
Available online 16 June 2011

Keywords:
CGRP
Extracellular loop
Receptor activation
Juxtamembrane domain
G protein-coupled receptor
Receptor activity-modifying protein

ABSTRACT

The first and third extracellular loops (ECL) of G protein-coupled receptors (GPCRs) have been implicated in ligand binding and receptor function. This study describes the results of an alanine/leucine scan of ECLs 1 and 3 and loop-associated transmembrane (TM) domains of the secretin-like GPCR calcitonin receptor-like receptor which associates with receptor activity modifying protein 1 to form the CGRP receptor. Leu195Ala, Val198Ala and Ala199Leu at the top of TM2 all reduced αCGRP-mediated cAMP production and internalization; Leu195Ala and Ala199Leu also reduced αCGRP binding. These residues form a hydrophobic cluster within an area defined as the "minor groove" of rhodopsin-like GPCRs. Within ECL1, Ala203Leu and Ala206Leu influenced the ability of αCGRP to stimulate adenylate cyclase. In TM3, His219Ala, Leu220Ala and Leu222Ala have influences on αCGRP binding and cAMP production; they are likely to indirectly influence the binding site for αCGRP as well as having an involvement in signal transduction. On the exofacial surfaces of TMs 6 and 7, a number of residues were identified that reduced cell surface receptor expression, most noticeably Leu351Ala and Glu357Ala in TM6. The residues may contribute to the RAMP1 binding interface. Ile360Ala impaired αCGRP-mediated cAMP production. Ile360 is predicted to be located close to ECL2 and may facilitate receptor activation. Identification of several crucial functional loci gives further insight into the activation mechanism of this complex receptor system and may aid rational drug design.

1. Introduction

The calcitonin receptor-like receptor (CLR) is a secretin-like (family B) G protein-coupled receptor (GPCR) protein that, in association with receptor activity modifying protein 1 (RAMP1), acts as a receptor for α and β calcitonin gene-related peptide (CGRP). αCGRP is a potent vasodilator with important pathophysiological actions especially in migraine. A structure of the N-termini of CLR and RAMP1 has recently been published [29]. RAMP1 and CLR dimerization is required for both ligand binding and cell surface expression [19] and CLR is also known to form an adrenomedullin receptor when it forms a heterodimer with either RAMP2 or RAMP3 [19]. A two-step model of receptor activation has been described for secretin-like GPCRs. Initially the C-terminus of the peptide ligand binds to the extracellular domain of the receptor. Then the N-terminus of the ligand associates with the transmembrane (TM) domain of the receptor including the extracellular loops (ECLs), leading to receptor activation [22]. Broadly, this generic model of receptor activation is likely to apply to the CGRP receptor although the important molecular details specific to αCGRP-binding remain unknown.

Within GPCRs, the ECLs contribute to receptor affinity and efficacy. They may also help orientate the TM bundle and provide key molecular determinants for ligand binding [23]. There is considerable evidence that the ECLs are important for the binding of peptide agonists to secretin-like GPCRs but the details may be receptor specific. Investigations into the parathyroid hormone 1 (PTH1) receptor using chimeric receptors and disulfide-trapping experiments suggest that the hormone has a diffuse pharmacophore making contact across all three ECLs, with the initial N-terminal serine residue positioned between TM5 and TM6 [2,21]. In the glucagon receptor, chimera and mutagenesis experiments also suggest the peptide is able to make extensive contacts across the extracellular TM domain, but the N-terminal residues are predicted to face ECL1 and TM2 [25]. In the secretin receptor, mutagenesis suggests contacts with ECL1 and ECL2, but a model based on photoaffinity cross-linking places the peptide largely in the vicinity of ECL3 [9,13]. Photoaffinity cross-linking data for the binding of GLP-1 suggests that it binds to ECL2 but closer to ECL1 [20].

The role of the ECLs in the CLR remains elusive. Consequently, an alanine scan has been used to investigate ECL1 and ECL3 and their

Abbreviations: AM, adrenomedullin; CGRP, calcitonin gene-related peptide; CLR, calcitonin receptor-like receptor; CT, calcitonin; ECD, extracellular domain; ECL, extracellular loop; ICL, intracellular loop; GPCR, G protein-coupled receptor; HA, hemagglutinin; PTH, parathyroid hormone; RAMP, receptor activity-modifying protein; RMSD, root mean squared deviation; TM, transmembrane domain; VPAC, vasoactive intestinal peptide receptor

* Corresponding author. Tel.: +44 121 204 3997; fax: +44 121 349 5142.
E-mail addresses: BarwellJ@aston.ac.uk (J. Barwell), A.C.Conner@warwick.ac.uk (A. Conner), D.R.Poyner@aston.ac.uk (D.R. Poyner).

0167-4889
doi:10.1016/j.bbamcr.2011.06.005

corresponding TM regions. Endogenous alanine residues within this region were substituted to leucine residues to probe the significance of the size and/or geometry of their methyl side chains. Mutant receptors were assessed on multiple criteria including cAMP production, agonist-mediated desensitization (which can provide an indirect measure of β-arrestin association [12]), cell-surface and total expression and human αCGRP binding in an attempt to determine the functional role of the residues within the protein.

2. Methods

2.1. Materials

Human αCGRP was from Calbiochem (Beeston, Nottingham, UK). ^{125}I-iodo^{8}histidyl-human αCGRP was from PerkinElmer Life and Analytical Sciences (Waltham, MA). [8-^{3}H] Adenosine 3′, 5′, cyclic phosphate, NH_4 salt was from Amersham Biosciences (Chalfont, UK). Chemicals were from Sigma-Aldrich UK. For ELISAs, the primary antibody was mouse, anti-HA antibody H9658 [Sigma-Aldrich], the secondary antibody was anti-mouse, horseradish peroxidase conjugated #7076 [Cell Signaling Technology] and *SIGMAFAST*™ o-phenylenediamine tablets were used.

2.2. Expression constructs and mutagenesis

The expression constructs used were human CLR with an N-terminal hemagglutinin (HA-CLR) epitope tag and human RAMP1 with an N-terminal *myc* epitope tag (*myc*-RAMP1) in pc DNA3.1(−). These were kindly provided by Dr. S. Foord. HA-CLR mutants were generated using the QuikChange II site-directed mutagenesis kit (Stratagene, Cambridge, UK), as described previously [3]. A snake plot showing the location of the residues mutated and other key features of the transmembrane domain of CLR is shown in Fig. 1.

2.3. Cell culture and transfection

Cos-7 cells were cultured and transfected with polyethyleneimine as described previously [27].

2.4. Radioligand binding

Radioligand binding using ^{125}I-iodo^{8}histidyl-human αCGRP on membranes prepared from transfected Cos-7 cells was as carried out by centrifugation as described previously [3]. The membrane concentration was 0.4 mg/ml.

2.5. Assay of cAMP production

48 well plates were transiently transfected with WT receptor (HA-CLR/*myc* RAMP1) alongside a mutant receptor in every experiment, to take account of day-to-day differences in transfection and coupling efficiencies. Stimulation with agonists and assay of cAMP was by a radioreceptor assay as described elsewhere [27].

2.6. Analysis of cell surface expression of mutants by ELISA and agonist dependent internalization

24 well plates were transiently transfected with WT receptor and a mutant receptor in every experiment. A negative control of *myc* RAMP1/empty pcDNA3.1(−) was used. To measure both cell surface and total expression of CLR an ELISA was carried out as described previously [5], but using the antibodies and o-phenylenediamine tablets described in the Materials section. A Biotek EL800 Universial Microplate reader using the 490 nm filter was used to quantify the peroxidise product. Cell surface expression data was normalized to make mean WT expression 100% and the mean *myc* RAMP1/empty pcDNA3.1(−) vector as 0%. Receptor internalization was measured after 1 h treatment with 100 nM human αCGRP at 37 °C by the above cell surface ELISA procedure.

2.7. Total CLR expression

Total WT and mutant receptor expression was only assessed on mutant receptors that were found to alter cell surface expression. The ELISA procedure outlined above was conducted but after the transfected cells were fixed with 3.7% formaldehyde for 15 min, the cells were permeabilized with 0.1% Triton X-100 in PBS for 1 h.

2.8. Construction of a CLR model to show the ECLs

Two CLR TM domain models were constructed. The putative TM segments of CLR were aligned against the TM domains in bovine rhodopsin (inactive, PDB 1U19) and opsin (active, PDB 3DQB) using the alignment proposed by Vohra and co-workers [30]. Modeller9v5 was used to generate 500 models. The models were ranked by Modeller9v5 energy objective function. The top 20 structures were retained and stereochemical quality was assessed by PROCHECKv3.5.4 [16,17]. Based on overall and residue-by-residue geometry a structure was selected.

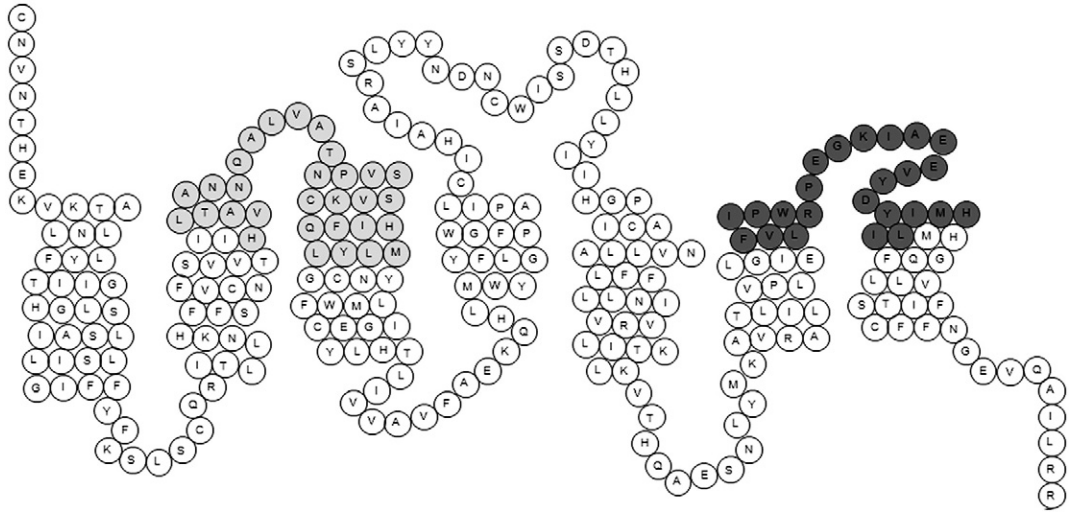

Fig. 1. Snake plot of transmembrane domain of CLR. Amino acids of CLR between 125 and 397 are depicted as circles containing 1-letter identifiers. The putative boundaries of the TM regions are shown. Residues that were mutated in the ECL1 and ECL3 regions are shaded.

The loop domains were constructed using the program Loopy [28,31] as described previously [1]. However, ECL2 was divided into two segments. Cys212 is assumed to participate in a highly conserved disulphide bond with Cys282. This was used as an anchor region. To model ECL2, the data of Conner and co-workers was used to select appropriate conformations [4].

The quality of the loop models was assessed by using the methodology to model ECL1 and ECL3 of bovine rhodopsin; these loops were then compared with those found in the crystal structure 1U19. The best ECL1 conformer had a 1.40 Å global root mean squared deviation from the crystal structure and the best ECL3 conformer had 0.74 Å. The mean and mode of the best top 10 conformers for ECL1 did not exceed 1.93 Å and 1.54 Å for ECL3.

The ProPka program [18] *via* the PDBQPR server [7] was used to assign the protonation states of the titratable groups in each CLR TM domain model, using the CHARMM parameters set at pH 7.4. The CLR TM models were then orientated on their Z-axis based on the relative position of Tyr165 and Tyr367. The CHARMM (c35b3) GBSW module containing the GB/SA membrane application was used [14]. The all-atom param22/cmap force-field in the presence of a 32 Å implicit membrane was set up. Then 1500 steps of a steepest descent energy minimization followed by 5000 steps of adopted basis Newton-Raphson minimization (or until the root mean squared deviation [RMSD] was less than 0.001 kcal/mol) was conducted. TM models contained an acetylated N-terminus and a N-methylamide C-terminus to prevent unnecessary large electrostatic attractive forces between the helical ends during energy minimization.

2.9. Statistical analysis of data

Curve fitting was completed by GraphPad Prism 4 as described previously [1]. A two-tailed independent *t*-test was used to determine significance between dose–response curve conditions. The Mann–Whitney *U* test was used to determine significance between conditions used in ELISA based assays. The analysis is indicated in the table and figure legends and has been described previously [1].

3. Results

3.1. Stimulation of cAMP production

Each mutant was challenged with human αCGRP and cAMP production was measured (Table 1, Figs. 2 and 3). For ECL1 a reduction in αCGRP potency (as assessed by significant differences in pEC_{50} values compared to WT receptors) was observed in the mutant receptors (in the order of the magnitude of EC_{50} fold decrease); Leu195Ala (~30 fold), Ala199Leu (~20 fold), Val198Ala (~11 fold), His219Ala (~11 fold) and Cys212Ala (~9 fold). In contrast, an increase in αCGRP potency was found in Leu220Ala (~25 fold), Ala203Leu (~11 fold), Ala206Leu (~9 fold) and Leu222Ala (~6 fold). In ECL3, Glu357Ala was found to significantly decrease pEC_{50} by ~33 fold compared to WT; this mutant also showed decreased maximal responses (41.7% ± 17.9%). Ile360Ala was also found to significantly decrease pEC_{50} by ~7 fold compared to WT.

Table 1
The ability of mutant receptors to stimulate cAMP compared to the WT receptor.

Mutant	N	pEC_{50} WT	pEC_{50} mutant	Mutant	N	pEC_{50} WT	pEC_{50} mutant
ECL1							
H194A	5	9.97 ± 0.48	9.41 ± 0.53	P209A	4	9.91 ± 0.33	9.85 ± 0.14
L195A	4	10.36 ± 0.25	8.87 ± 0.09**	V210A	4	9.95 ± 0.29	10.44 ± 0.23
T196A	3	9.73 ± 0.21	10.18 ± 0.10	S211A	4	9.49 ± 0.33	9.60 ± 0.21
A197L	4	10.09 ± 0.29	10.05 ± 0.39	C212A	3	9.71 ± 0.28	8.78 ± 0.18*
V198A	5	9.67 ± 0.17	8.87 ± 0.26*	K213A	5	9.49 ± 0.40	8.78 ± 0.39
A199L	6	10.20 ± 0.31	8.87 ± 0.32*	V214A	4	9.83 ± 0.39	9.97 ± 0.37
N200A	3	9.80 ± 0.17	9.62 ± 0.28	S215A	6	9.39 ± 0.33	9.41 ± 0.22
N201A	4	9.38 ± 0.16	9.88 ± 0.29	Q216A	3	9.63 ± 0.13	9.94 ± 0.13
Q202A	4	9.49 ± 0.43	9.17 ± 0.32	F217A	4	9.94 ± 0.43	9.37 ± 0.22
A203L	5	9.75 ± 0.22	10.77 ± 0.35*	I218A	4	9.27 ± 0.22	9.60 ± 0.25
L204A	3	9.73 ± 0.13	9.68 ± 0.17	H219A	3	9.41 ± 0.17	8.35 ± 0.13**
V205A	4	9.62 ± 0.21	10.04 ± 0.30	L220A	4	9.53 ± 0.17	10.93 ± 0.13***
A206L	5	9.43 ± 0.29	10.37 ± 0.19*	Y221A	4	9.73 ± 0.42	9.01 ± 0.51
T207A	4	9.98 ± 0.30	10.50 ± 0.20	L222A	5	9.95 ± 0.21	10.75 ± 0.10*
N208A	3	9.85 ± 0.11	9.97 ± 0.18	M223A	4	9.71 ± 0.18	9.65 ± 0.15
ECL3							
F349A	4	10.59 ± 0.34	10.72 ± 0.28	Y367A	4	9.64 ± 0.21	9.92 ± 0.04
V350A	3	9.89 ± 0.02	9.74 ± 0.15	I368A	5	10.13 ± 0.33	10.30 ± 0.22
L351A	3	9.36 ± 0.16	9.54 ± 0.04	M369A	4	9.92 ± 0.32	10.53 ± 0.39
I352A	6	10.00 ± 0.36	9.33 ± 0.15	H370A	5	9.42 ± 0.14	9.19 ± 0.30
P353A	5	9.79 ± 0.27	9.06 ± 0.21	I371A	4	9.96 ± 0.28	10.18 ± 0.20
W354A	4	9.08 ± 0.36	8.91 ± 0.28	L372A	3	9.93 ± 0.07	10.08 ± 0.26
R355A	4	9.86 ± 0.37	9.55 ± 0.21	M373A	3	10.51 ± 0.28	10.21 ± 0.12
P356A	3	10.39 ± 0.42	9.95 ± 0.26	E362A	3	9.70 ± 0.26	9.65 ± 0.33
E357A	4	10.44 ± 0.46	8.92 ± 0.39**	E363A	4	10.32 ± 0.49	9.80 ± 0.32
G358A	3	9.68 ± 0.31	9.46 ± 0.29	V364A	3	9.78 ± 0.22	9.94 ± 0.15
K359A	4	9.76 ± 0.12	9.94 ± 0.32	Y365A	4	10.20 ± 0.27	10.33 ± 0.25
I360A	6	9.26 ± 0.14	8.40 ± 0.22**	D366A	3	9.54 ± 0.21	9.72 ± 0.21
A361L	7	9.97 ± 0.22	10.27 ± 0.22	Y367A	4	9.64 ± 0.21	9.92 ± 0.04
E362A	3	9.70 ± 0.26	9.65 ± 0.33	I368A	5	10.13 ± 0.33	10.30 ± 0.22
E363A	4	10.32 ± 0.49	9.80 ± 0.32	M369A	4	9.92 ± 0.32	10.53 ± 0.39
V364A	3	9.78 ± 0.22	9.94 ± 0.15	H370A	5	9.42 ± 0.14	9.19 ± 0.30
Y365A	4	10.20 ± 0.27	10.33 ± 0.25	I371A	4	9.96 ± 0.28	10.18 ± 0.20
D366A	3	9.54 ± 0.21	9.72 ± 0.21	L372A	3	9.93 ± 0.07	10.08 ± 0.26

Values are pEC_{50} means ± S.E.M. pEC_{50} mutant values were compared to WT using an independent two-tailed *t*-test.
* $p<0.05$.
** $p<0.01$.
*** $p<0.001$.

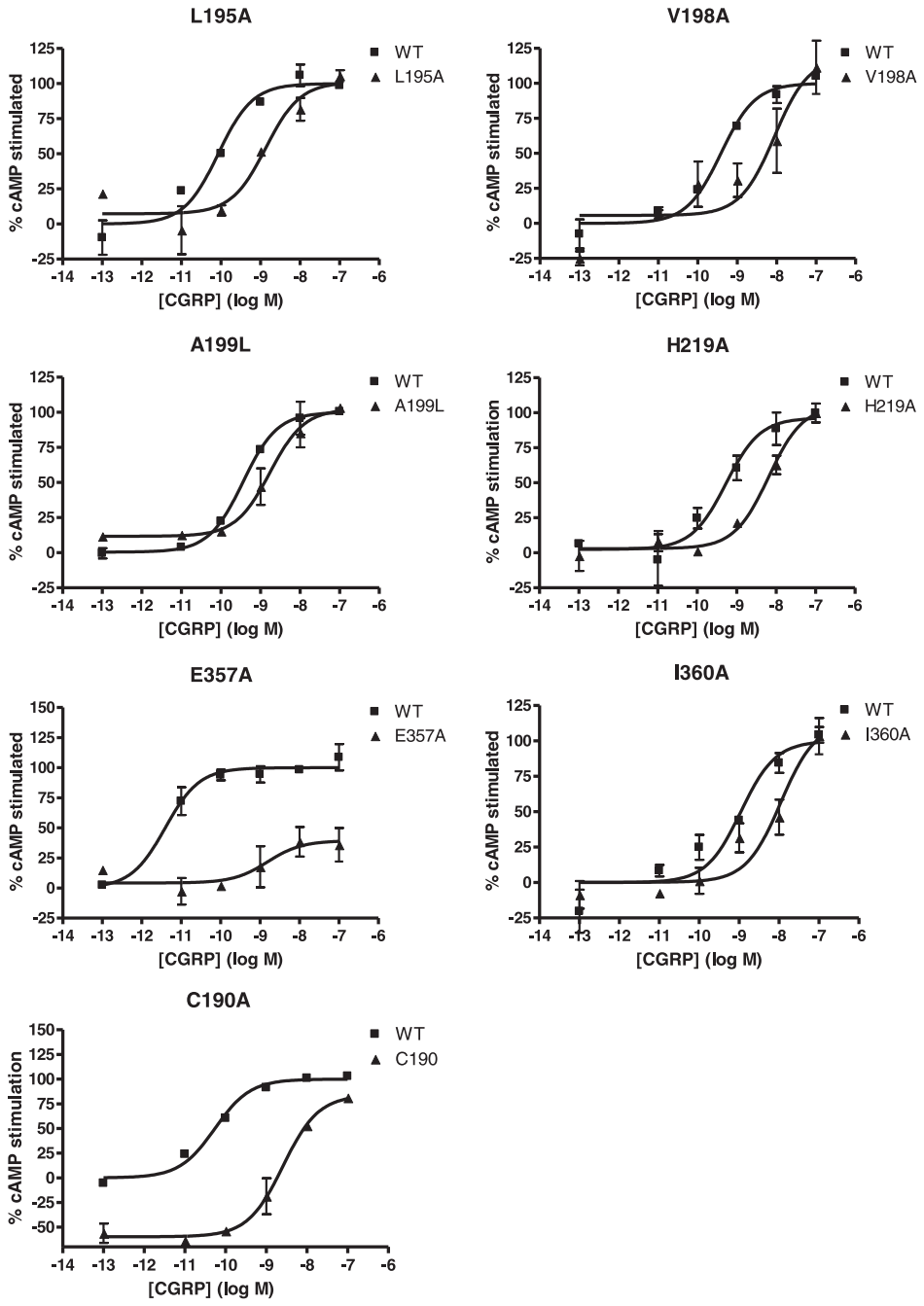

Fig. 2. Representative dose–response curves of ECL mutants that showed a significant decrease in αCGRP potency for cAMP production. Sigmoidal concentration–response curves comparing the WT receptor and mutant receptors are shown. Each WT and mutant receptor concentration–response comparison curve is a representative example from at least three independent experiments. Each assay point was performed in duplicate where each point on the graph represents the mean ± S.E.M.

For a number of mutants, there were changes in either basal activity or maximum response. However, in most cases these were small (Table 2). There were ~40% increases in maximum response for Leu204Ala and Gln216Ala in ECL1 and for Val350Ala, Arg355Ala, Ala361Leu and Met369Ala in ECL3. For Leu204Ala and Arg355Ala there was also a ~30% increase in basal activity; Pro209Ala and Val210Ala had a similar increase in this parameter.

3.2. Cell surface receptor expression

Expression of receptors was measured using a cell-surface ELISA (Table 3). Statistically significant reductions in cell-surface expression were seen in nine mutants in ECL1. The largest reduction in cell surface expression was with Met223Ala (~40%) but overall the cell surface reductions seen in these mutants were fairly modest, although four consecutive mutants (Phe217Ala, Ile218Ala, His219Ala and Leu220Ala) reduced cell surface expression. Four mutants in ECL1 were found to increase cell surface expression significantly, but the effect was not much more than a 30% increase (Table 3). By contrast, in ECL3 there were large decreases in expression for Glu357Ala and Leu351Ala (>70%). Gly358Ala, Tyr356Ala and Tyr367Ala showed decreases of around 40%. There were smaller changes in a further seven mutants (see Table 3). An increase in cell surface expression was found in His370Ala (of 41%) and Pro353Ala (33%).

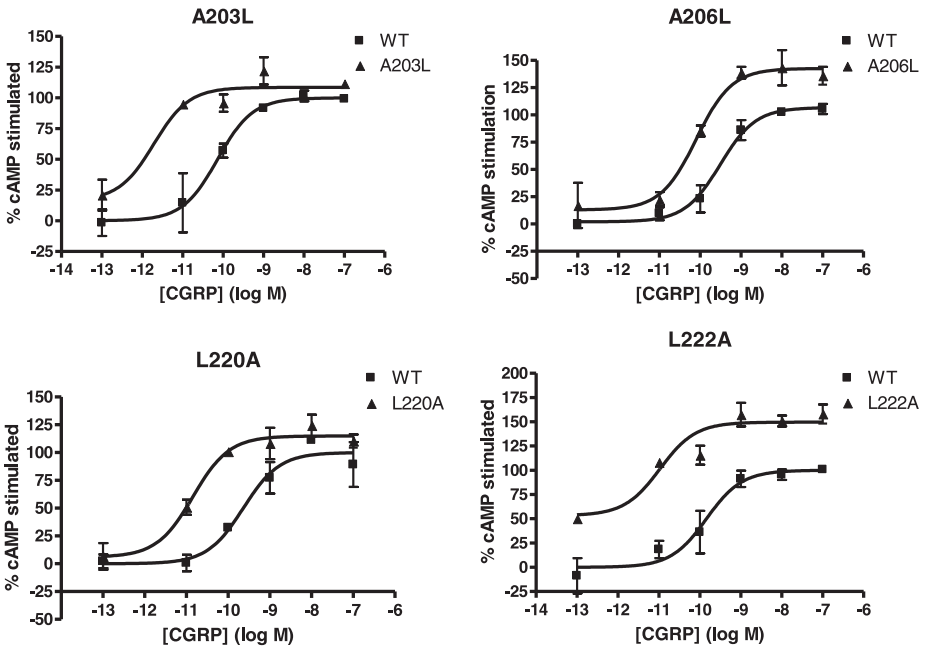

Fig. 3. Representative dose–response curves of mutants that showed a significant increase in αCGRP potency. Sigmoidal concentration–response curves comparing the WT receptor and mutant receptors are shown. Each WT and mutant receptor concentration–response comparison curve is a representative example from at least three independent experiments. Each assay point was performed in duplicate where each point on the graph represents the mean ± S.E.M.

3.3. Total receptor expression

Total receptor expression probing for the HA epitope was assessed on mutant receptors that were either found to have a significantly different pEC_{50} and/or cell surface expression. For residues in ECL1, a significant, yet modest, increase in total expression was observed in Val205Ala and Ala206Leu. A significant decrease in total expression was seen in Cys212Ala and His219Ala but again the size of the effect was only modest (Table 4). For ECL3, a significant 44% increase in total expression compared to WT was observed in Pro353Ala. A significant

Table 2
Mutant receptors showing large changes in mean basal activity and E_{max}.

Mutant	N	Mean basal activity (% WT)	Mean E_{max} (% WT)
ECL1			
L204A	3	37.3 ± 18.5	142.3 ± 13.4
P209A	4	41.5 ± 5.2	122.5 ± 5.0
V210A	4	33.7 ± 8.9	117.9 ± 10.7
C212A	3	−6.7 ± 33.3	130.2 ± 23.8
Q216A	3	22.7 ± 8.1	144.0 ± 13.7
M223A	4	13.2 ± 11.1	128.8 ± 16.2
T207A	4	0.4 ± 7.7	122.5 ± 9.3
ECL3			
F349A	4	10.3 ± 6.0	122.1 ± 6.8
V350A	3	19.3 ± 5.8	142.3 ± 14.6
I352A	6	25.8 ± 5.3	121.1 ± 8.9
R355A	4	39.7 ± 11.2	151.5 ± 10.9
K359A	4	12.6 ± 14.6	121.7 ± 11.1
A361L	7	15.6 ± 8.2	146.2 ± 12.7
E363A	4	7.6 ± 9.5	127.5 ± 6.5
Y365A	4	22.5 ± 1.3	119.7 ± 6.0
Y367A	4	16.9 ± 11.2	123.2 ± 6.0
M369A	4	19.2 ± 6.7	139.5 ± 12.9

The WT and mutant cAMP dose–response comparison curves were normalized from 0% to 100% based on WT Top and Bottom values generated by GraphPad Prism 4. The E_{max} and basal activity of each mutant was assessed by the mean of the top and bottom of each dose–response curve. The mutant receptors mean E_{max} and basal activity was expressed as a percentage that corresponded to WT normalization. A difference was noted if the mean size of effect differed by 20% or more. Values reported are mutant percent means ± S.E.M. (% WT).

Table 3
Cell surface expression of mutant receptors.

Mutant	Cell surface expression (% WT)	Mutant	Cell surface expression (% WT)
ECL1			
H194A	106.5 ± 9.9	P209A	133.0 ± 9.0*
L195A	92.7 ± 5.4	V210A	111.9 ± 12.4
T196A	96.0 ± 9.2	S211A	92.62 ± 11.6
A197L	88.2 ± 5.3	C212A	69.71 ± 10.3*
V198A	133.4 ± 11.6***	K213A	94.54 ± 9.1
A199L	130.2 ± 8.2**	V214A	88.17 ± 8.9
N200A	74.8 ± 6.0*	S215A	101.6 ± 6.8
N201A	91.0 ± 8.3	Q216A	107.3 ± 8.4
Q202A	81.4 ± 11.9	F217A	72.78 ± 6.7*
A203L	112.4 ± 6.9	I218A	73.05 ± 8.4**
L204A	105.9 ± 5.6	H219A	68.81 ± 7.2***
V205A	81.3 ± 3.3	L220A	79.21 ± 6.1*
A206L	114.5 ± 4.9**	Y221A	107.3 ± 9.9
T207A	111.6 ± 11.5	L222A	94.33 ± 9.6
N208A	68.88 ± 7.3**	M223A	58.97 ± 8.3***
ECL3			
F349A	69.0 ± 7.0*	A361L	71.3 ± 11.0
V350A	78.9 ± 5.9	E362A	83.8 ± 5.8*
L351A	27.2 ± 4.4***	E363A	89.6 ± 11.9
I352A	70.5 ± 4.6***	V364A	135.3 ± 18.5
P353A	133.3 ± 11.8**	Y365A	60.0 ± 8.7**
W354A	88.1 ± 4.7*	D366A	85.9 ± 4.9*
R355A	66.2 ± 5.5**	Y367A	56.6 ± 4.9***
P356A	85.0 ± 6.0	I368A	129.0 ± 11.5
E357A	11.0 ± 3.5***	M369A	99.9 ± 4.8
G358A	61.4 ± 11.2*	H370A	141.1 ± 9.5***
K359A	71.8 ± 5.8***	I371A	70.5 ± 7.6**
I360A	107.7 ± 8.0	L372A	102.3 ± 13.0

Cell surface expression ELISA was used to probe for the presence of the HA epitope. Mutant HA CLR/*myc* RAMP1 receptors were compared with WT HA CLR/*myc* RAMP1 receptors. 3–6 independent experiments that contained triplicate data points were used in analysis. The raw data for each independent experiment was normalized where the mean WT receptor cell-surface expression equalled a 100% and the mean negative control (*myc* RAMP1/empty pcDNA3.1−) was equal to 0%. Values reported are mutant means ± S.E.M. (% WT). Mutant cell surface expression was compared to WT receptor using a Mann–Whitney *U* test.

* $p<0.05$.
** $p<0.01$.
*** $p<0.001$.

Table 4
Total expression of mutant receptors.

Mutant	Total expression (% WT mean ± S.E.M.)	Mutant	Total expression (% WT mean ± S.E.M.)
ECL1			
L195A	111.5 ± 8.5	P209A	106.8 ± 5.3
V198A	87.6 ± 13.5	C212A	80.0 ± 7.9*
A199L	115.5 ± 5.6	F217A	98.9 ± 6.0
N200A	104.8 ± 7.3	I218A	118.2 ± 12.7
A203L	110.2 ± 8.5	H219A	75.7 ± 16.5***
V205A	115.0 ± 4.8*	L220A	101.6 ± 4.7
A206L	116.5 ± 3.1**	L222A	106.4 ± 6.0
N208A	110.4 ± 3.8	M223A	101.7 ± 6.2
ECL3			
L351A	111.0 ± 12.4	I360A	89.5 ± 2.9
I352A	98.9 ± 10.3	A361L	87.2 ± 4.7
P353A	144.0 ± 12.3 ***	Y365A	116.0 ± 15.2
W354A	103.5 ± 5.3	D366A	78.2 ± 4.8**
R355A	110.9 ± 10.9	I368A	104.1 ± 10.9
E357A	88.6 ± 7.5	H370A	144.3 ± 6.8
G358A	92.9 ± 4.2	I371A	126.9 ± 12.7

Total expression of HA-tagged receptors both mutant and WT were analyzed when co-transfected with *myc* RAMP1 using an ELISA. At least 3 independent experiments containing triplicate data points were used in analysis. Total expression in the mutant condition was normalized to the WT condition (equal to 100%) and negative control (myc RAMP1/empty pcDNA3.1− after 0.1% Triton X-100, which was equal to 0%). A Mann–Whitney *U* test was used to assess statistical differences between WT and mutant receptors.

* $p<0.05$.
** $p<0.01$.
*** $p<0.001$.

Table 6
Apparent affinities of αCGRP for ECL mutant receptors that show a change in internalization or pEC_{50} for cAMP production, estimated by inhibition of radioligand binding.

Mutant	N	pIC_{50} for WT receptor (mean ± S.E.M.)	pIC_{50} for mutant receptors (mean ± S.E.M.)
ECL1			
L195A	5	9.01 ± 0.40	N.M.B.
V198A	4	8.86 ± 0.40	8.07 ± 0.47
A199L	4	8.88 ± 0.25	7.26 ± 0.13**
A203L	4	9.33 ± 0.31	9.77 ± 0.64
A206L	5	9.00 ± 0.13	9.19 ± 0.19
N208A	5	9.03 ± 0.09	8.90 ± 0.21
C212A	4	9.04 ± 0.09	6.94 ± 0.49**
H219A	4	9.01 ± 0.07	7.91 ± 0.44
L220A	5	9.36 ± 0.20	10.21 ± 0.36
L222A	3	9.84 ± 0.03	10.76 ± 0.17**
ECL3			
L351A	4	9.04 ± 0.36	N.M.B.
P353A	7	9.18 ± 0.33	8.65 ± 0.24
E357A	3	9.84 ± 0.03	N.M.B
I360A	3	8.77 ± 0.09	7.83 ± 0.33
W354A	4	9.01 ± 0.12	8.75 ± 0.13
E362A	3	9.05 ± 0.04	8.74 ± 0.18
I371A	3	9.84 ± 0.03	10.16 ± 0.11*

Mean ± S.E.M. pIC_{50} WT and mutant values shown. An independent two-tailed *t*-test was used to assess statistical differences. N.M.B., no measurable binding.

* $p<0.05$.
** $p<0.01$.

Table 5
Mutant receptors capability of agonist (αCGRP) mediated internalization compared to the WT receptor.

Mutant	WT receptor internalization (% mean ± S.E.M.)	Mutant receptor internalization (% mean ± S.E.M.)	Mutant	WT receptor internalization (% mean ± S.E.M.)	Mutant receptor internalization (% mean ± S.E.M.)
ECL1					
H194A	47.70 ± 4.9	58.14 ± 4.7	P209A	55.38 ± 5.8	55.90 ± 6.3
L195A	53.99 ± 2.8	1.67 ± 3.2***	V210A	62.01 ± 4.1	61.18 ± 6.0
T196A	51.98 ± 5.5	67.44 ± 3.2	S211A	54.01 ± 3.1	58.33 ± 2.8
A197L	54.66 ± 2.9	52.04 ± 3.6	C212A	58.04 ± 4.7	37.29 ± 9.7*
V198A	55.52 ± 3.0	30.32 ± 3.7***	K213A	52.00 ± 4.5	51.53 ± 6.1
A199L	64.04 ± 4.1	8.39 ± 7.7***	V214A	46.50 ± 2.9	59.87 ± 5.4
N200A	58.81 ± 3.0	67.90 ± 5.6	S215A	66.03 ± 7.2	64.07 ± 5.1
N201A	56.81 ± 3.9	63.03 ± 2.8	Q216A	50.47 ± 2.5	55.27 ± 3.3
Q202A	60.38 ± 4.9	66.48 ± 8.2	F217A	45.10 ± 8.0	44.78 ± 7.4
A203L	56.37 ± 4.0	62.21 ± 3.3	I218A	48.68 ± 8.5	66.06 ± 9.8
L204A	47.72 ± 5.2	49.54 ± 4.3	H219A	55.42 ± 3.1	75.07 ± 6.9*
V205A	51.32 ± 7.4	64.42 ± 4.0	L220A	55.44 ± 3.3	58.27 ± 4.5
A206L	56.97 ± 2.0	61.03 ± 2.2	Y221A	51.50 ± 4.6	63.57 ± 4.1
T207A	53.11 ± 2.1	58.75 ± 10.3	L222A	48.54 ± 7.0	56.60 ± 7.6
N208A	47.87 ± 5.3	65.65 ± 3.1*	M223A	48.32 ± 3.2	60.59 ± 4.5
ECL3					
F349A	70.16 ± 4.8	62.83 ± 3.5	A361L	78.82 ± 6.7	66.22 ± 10.7
V350A	61.22 ± 8.2	48.00 ± 6.7	E362A	49.11 ± 2.1	58.16 ± 2.3**
L351A	57.34 ± 4.0	19.84 ± 7.5***	E363A	68.34 ± 4.2	67.59 ± 2.8
I352A	60.98 ± 3.8	55.03 ± 6.2	V364A	68.87 ± 9.2	59.00 ± 7.2
P353A	74.76 ± 1.8	58.80 ± 1.8***	Y365A	68.69 ± 4.8	76.69 ± 4.0
W354A	73.25 ± 1.8	57.26 ± 2.7***	D366A	48.38 ± 2.6	51.89 ± 5.2
R355A	57.71 ± 6.7	60.95 ± 6.9	Y367A	57.35 ± 4.2	60.54 ± 5.8
P356A	65.78 ± 5.7	76.63 ± 4.8	I368A	64.42 ± 8.3	73.82 ± 3.5
E357A	57.13 ± 3.7	8.589 ± 6.3***	M369A	64.77 ± 4.4	67.48 ± 2.8
G358A	60.09 ± 6.7	73.04 ± 10.2	H370A	56.94 ± 6.3	51.04 ± 5.2
K359A	52.46 ± 2.7	59.11 ± 4.7	I371A	56.49 ± 6.0	82.69 ± 3.4**
I360A	71.00 ± 2.2	71.55 ± 2.2	L372A	53.99 ± 4.4	62.33 ± 5.4

Agonist mediated internalization of the CGRP receptor (both WT and mutant receptors) was approximated by a HA epitope probing cell surface ELISA taking into account the difference in cell surface expression levels between CGRP receptors that have or have not been exposed to 100 nM of human αCGRP for an 1 h. Percent mean ± S.E.M. agonist mediated internalization was determined by 3–6 independent experiments that contained triplicate data points. A Mann–Whitney *U* test was used to compare mutant and WT percent agonist internalization.

* $p<0.05$.
** $p<0.01$.
*** $p<0.001$.

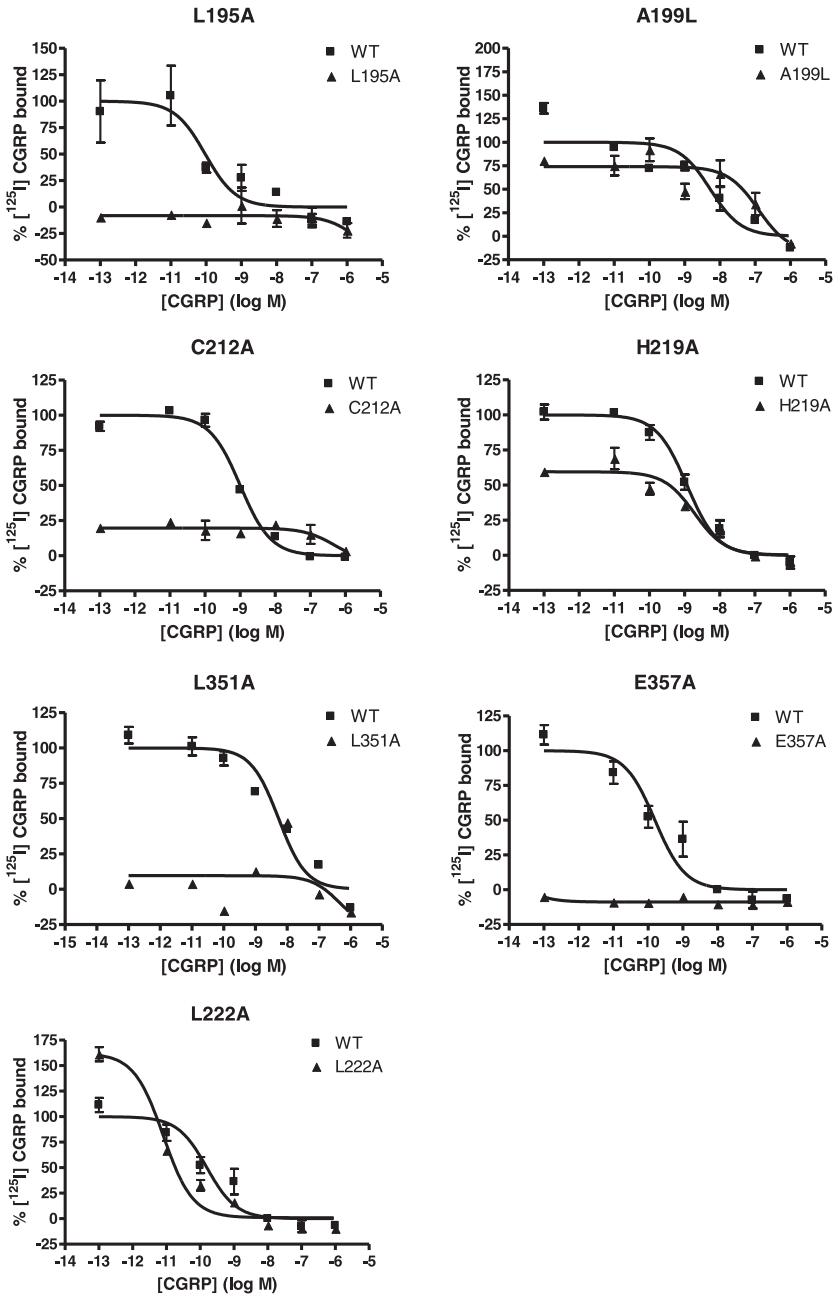

Fig. 4. Representative inhibition curves of ECL mutant receptors that significantly alter CGRP binding. Sigmoidal αCGRP inhibition curves comparing the WT receptor and mutant receptors are shown. Each WT and mutant receptor curve is a representative example of at least three independent experiments. Each assay point was performed in duplicate where each point on the graph represents the mean ± S.E.M.

but modest decrease (22%) in total expression was observed in Asp366Ala.

3.4. αCGRP mediated internalization

In ECL1, αCGRP mediated internalization was severely impaired or abolished in Leu195Ala and Ala199Leu and significantly reduced in Cys212Ala and Val198Ala. In contrast, Asn208Ala and His219Ala were found to internalize moderately more readily than WT (Table 5).

For ECL3, internalization was severely impaired by Glu357Ala and significantly reduced in Leu351Ala, Pro353Ala and Trp354Ala. In contrast, Glu362Ala and Ile371Ala were found to internalize more readily than WT (Table 5).

3.5. Inhibition of ^{125}I-αCGRP radioligand binding

The ability of αCGRP to displace ^{125}I-αCGRP was investigated on mutant receptors that were either found to have a significantly different mean pEC_{50} and/or agonist-mediated internalization when compared to WT (see Table 6, Fig. 4). For ECL1, the pIC_{50} of four mutants were significantly reduced when compared to WT; Leu195Ala, Ala199Leu, Cys212Ala and His219Ala. In contrast, the pIC_{50} of Leu200Ala showed an increase compared to WT. For ECL3, the mean pIC_{50} of two mutants were significantly reduced; Leu351Ala and Glu357Ala. The decrease for Ile360Ala approached significance ($p = 0.052$). Contrastingly, the pIC_{50} of Ile371Ala showed a small increase compared to WT.

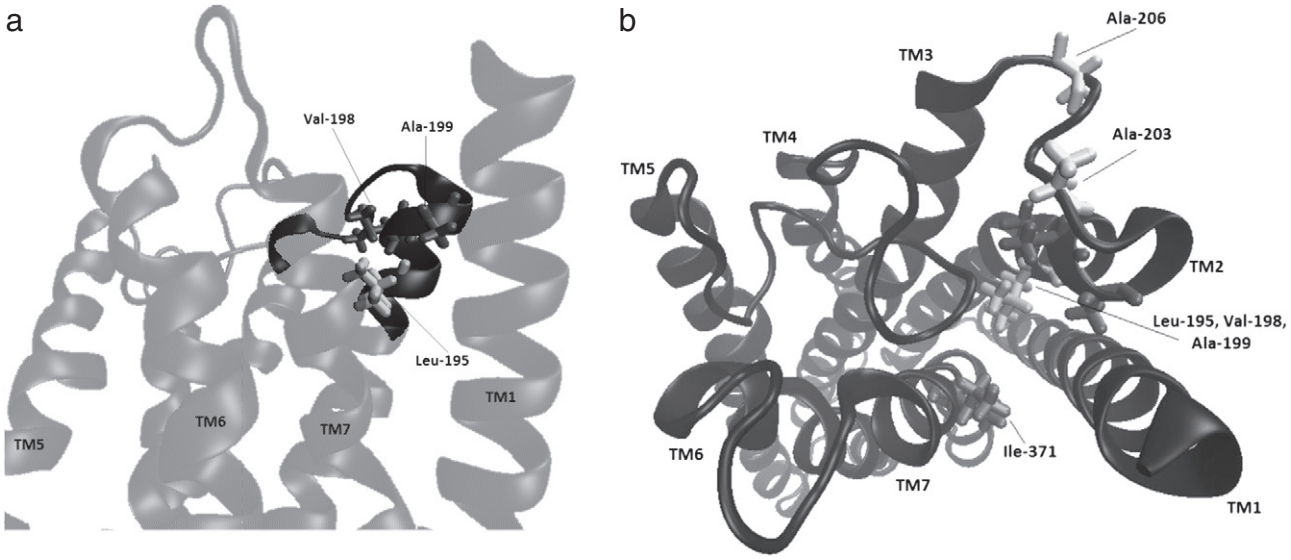

Fig. 5. Important residues affiliated with the TM1–TM2–TM7 region of CLR. a) Side view of the CLR TM domain model generated from bovine rhodopsin (PDB accession code 1U19) showing the relative position of Leu195, Val198 and Ala199. A transparent ribbon represents the TM helical arrangement, where TM1, 5, 6 and 7 have been labeled. ECL1 and associated TM2 is highlighted by an opaque ribbon. b) Extracellular view of the CLR TM model (PDB accession code 1U19) represented by transparent ribbon with depth cue perception. Ile371 is located within TM7. Ala203 and Ala206 are predicted to be in the middle of ECL1. Leu195, Val198 and Ala199 are located at the top of TM2.

3.6. ECL1 and ECL3 in the CLR model

The models of CLR are shown in Figs. 5, 6 and 7. A number of important features can be noted. In ECL1, Leu195, Val198 and Ala199 residues when mutated, impaired normal CGRP receptor pharmacology but still expressed at the cell surface are predicted to form a cluster at the top of TM2 and are close to the N-terminal segment of ECL2. They are also close to Ile371 of TM7, which showed enhanced internalization and a small increase in affinity for αCGRP upon mutation. Ala203 and Ala206, which on mutation increased αCGRP potency, are predicted to be at the top of ECL1. His219Ala, Leu220Ala and L222Ala all influenced αCGRP efficacy and the residues are predicted to be located in the middle of TM3. Leu351Ala, Arg355Ala, Glu357Ala, Gly358Ala, Lys359Ala, Glu362Ala, Tyr365Ala, Tyr367Ala and Ile371Ala were found to decrease cell surface expression and they are all predicted to be located across TM6, ECL3 and TM7. These residues are predicted to face outwards toward the supposed lipid environment (Fig. 7).

4. Discussion

Currently, it is unclear how extracellular loops in Secretin-like GPCRs contribute to receptor functioning. A systematic alanine/leucine scan was conducted on ECL1 and ECL3 of CLR and their corresponding juxtamembrane regions. Mutant CGRP receptors were assessed on multiple criteria including; cAMP accumulation, cell surface expression, total expression, agonist mediated internalization and αCGRP radioligand binding. This approach found that both regions of the receptor are required for

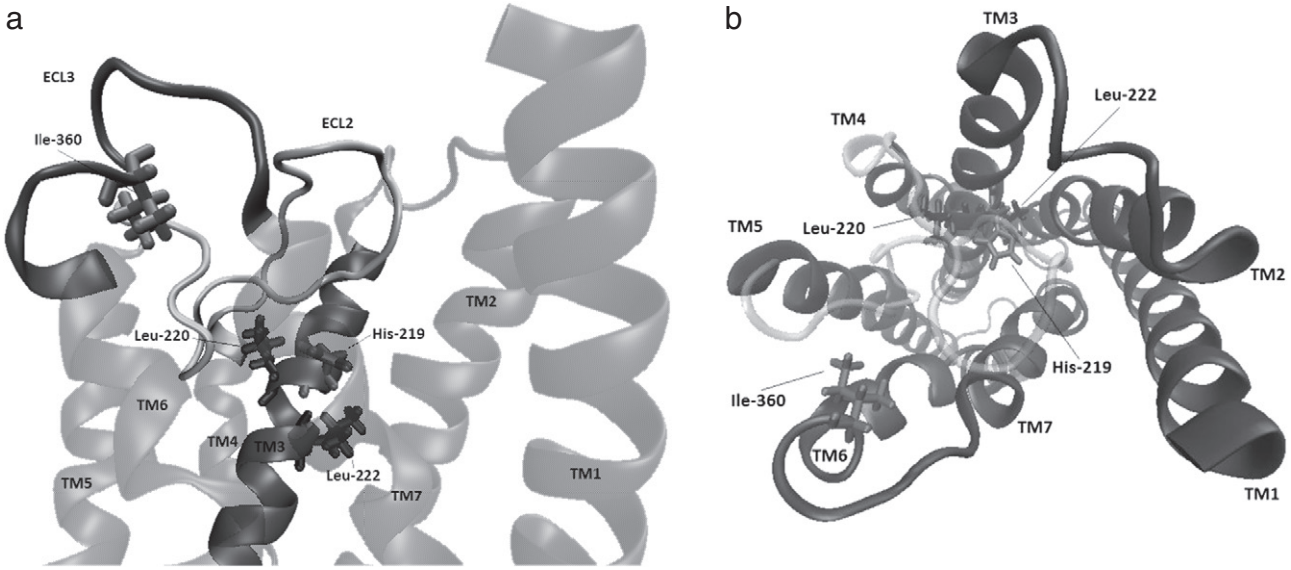

Fig. 6. Predicted location of H219, L220, L222 and I360. a) Side view of the CLR TM domain model generated from bovine rhodopsin (PDB accession code 3DQB) represented by transparent ribbon. TM3, ECL3 and ECL2 are opaque ribbons. His219, Leu220 and Leu222 are located within TM3. Ile360 is located within ECL3 in close proximity to ECL2. b) Extracellular view of the CLR TM model. ECL2 is transparent. The same residues as above are shown.

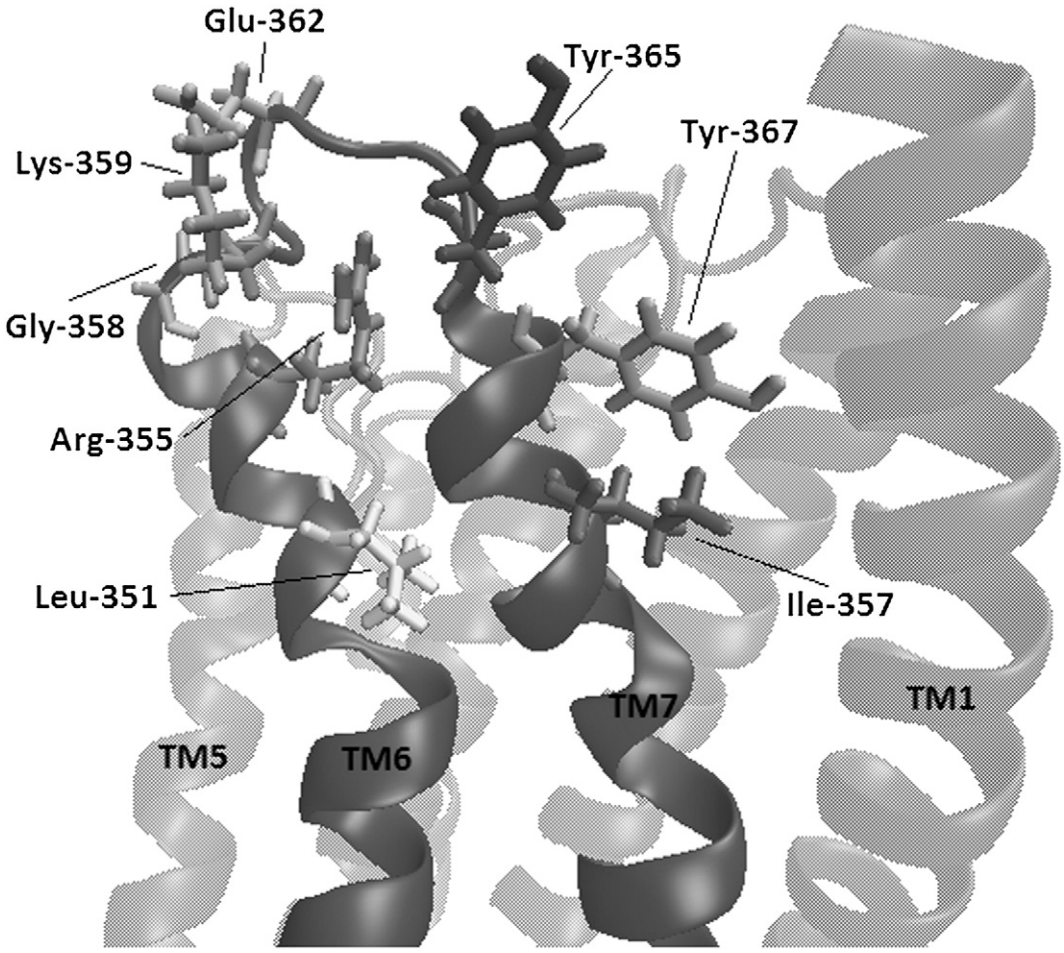

Fig. 7. Putative RAMP1 interface. Side view of the CLR TM domain model generated from bovine rhodopsin (PDB accession code 3DQB) represented by transparent ribbons. TM6 and TM7 highlighted by opaque ribbons. The side chains of Leu351, Arg355, Gly358, Lys359, Glu362, Tyr365, Tyr367 and Ile357 are highlighted to represent residues that were found to reduce cell surface expression and predicted in this model to face outward toward the supposed lipid environment.

normal receptor pharmacology and has revealed key molecular determinants that facilitate receptor activation.

A cluster of three residues, Leu195, Val198 and Ala199 that are located at the top of TM2 and predicted to face into the TM bundle (Fig. 5) are required for CGRP receptor function. Both Leu195 and Ala199 disrupted CGRP binding when mutated, thereby providing a likely explanation of their effects. Leu195 and Ala199 may directly participate in the orthosteric binding site or the mutations could indirectly impair αCGRP binding (e.g. disrupt helical packing or water–lipid interface). The hydrophobic triplet cluster is predicted to be between TM1, 2 and 7. Within rhodopsin-like GPCRs, this region of the receptor has been termed the "minor groove" when considering ligand binding and it has been suggested that it is important for activation, particularly of beta-arrestin [24]. Interestingly Ile371, which is predicted to be in close proximity to the groove, increased CGRP receptor internalization when mutated to alanine, possibly reflecting better association of the receptor with β-arrestin. It is not known if a minor groove exists in secretin-like GPCRs, but there is evidence that the region is important. In the family B receptors, the consensus residue at Leu195 is actually an aspartate, which is part of a Lys/ArgGluArg motif found in 10/15 of human secretin-like GPCRs (Supplementary Fig. 1). Langer et al., [15] found that mutating this motif reduced the ability of the VPAC1 receptor to stimulate cAMP production. This observation is in line with previous studies on the VPAC1 receptor [10] and the secretin receptor [6]. Although primary sequence is not conserved, these observations support the importance of this region in secretin-like GPCRs. There is evidence that small-molecule calcitonin agonists interact with residues at the exofacial end of TM1 [8]. This again suggests the plausibility of a molecular switch necessary for activation within this region of the receptor.

Within ECL1 itself, Ala203Leu and Ala206Leu were found to increase the potency of αCGRP in its ability to stimulate cAMP. It is plausible that the introduced leucines assist αCGRP docking into the TM domain, although the mechanism behind this is unknown. At the very base of ECL1, mutation of Cys212 severely impaired receptor function, consistent with its involvement in a disulfide bond with C282 located in ECL2; a highly conserved feature of all GPCRs.

A cluster of three residues is predicted to be located in the middle of TM3 (Fig. 6). His219Ala reduced total and cell surface expression and cAMP production. However the receptor showed a small increase in agonist mediated internalization, possibly suggesting an increase in coupling to β-arrestin. Leu220Ala and Leu222Ala increased the potency of αCGRP in stimulating cAMP production and Leu222Ala was found to significantly enhance αCGRP binding. In rhodopsin-like GPCRs, TM3 is crucial for receptor activation and these residues may define a portion of the helix that is important for mediating conformational changes in CLR [32]. Models of CLR based on different activity states of rhodopsin suggested that TM3 in CLR might undergo a subtle rotational movement upon activation, which changes the relative positions of His219, Leu220 and Leu222. This is very speculative, but given that there are some shared features in the activation mechanisms of rhodopsin- and secretin-like GPCRs [3,26],

this cluster of residues is in an excellent position to take part in inter-helical interactions. Yet, it cannot be ruled out that αCGRP may directly influence this cluster of residues. Cross-linking data indicates that the N-terminus of PTH is in close proximity to Phe424 of the PTH1 receptor [21]; in our model of CLR, the equivalent to this residue (Ile352, discussed below), is at a similar level in the helical bundle to Leu220 (see Supplementary Fig. 2). Thus it remains plausible that αCGRP may penetrate deep within the juxtamembrane domain.

Within the predicted ECL3 (Fig. 7), Ile360Ala had major effects on CGRP potency. This is predicted to be in the center of ECL3, in close proximity to ECL2. It significantly reduced cAMP production. It is reasonable to speculate that Ile360 contributes either directly to the signal transduction process mediated by αCGRP or participates indirectly by stabilizing ECL2.

Half of the mutants in ECL3 and the associated juxtamembrane regions reduced cell surface expression of the CGRP receptor but had no effect on total receptor expression. Glu357 in ECL3 and Leu351, deep in TM6, are particularly important for normal CGRP receptor cell surface expression. Experimental evidence has shown that RAMP3 dimerized with the secretin receptor at TM6 and TM7 [11]; a result consistent with an earlier prediction from evolutionary trace analysis [30]. Most of the residues, which were found to have a decrease in cell surface expression, are predicted to be located across TM6, ECL3 and TM7 with their side-chains facing outwards toward the lipid environment (Fig. 7), although some intra-helical packing effects cannot be ruled as Glu357 is predicted in the inactive model to associate with TM5. The modeling is speculative as the rhodopsin template used for this is not truly representative, although we have used it to successfully predict the effects of mutations in TM6 [3]. However, given these limitations, the model predicts the mutations identified could theoretically participate in a RAMP1 interface disrupting the efficiency of CLR and RAMP1 dimerization. RAMP1 is a chaperone protein and its association to CLR is essential for CGRP receptor trafficking to the cell surface [19].

Given that movements of TM6 are needed for GPCR activation [3,32] it is interesting that a cluster of residues at the TM6–TM7 interface (Ile352Ala, Arg355Ala, Lys359Ala, Tyr365Ala and Tyr367Ala) are associated with increases in either basal activity or maximum response on mutation. Within the PTH receptor, Leu368, Tyr421 and Phe424 have been shown to be in close proximity to the N-terminus of bound PTH [21] and so may be involved in agonist-mediated conformational changes; Phe424 of the PTH receptor is the equivalent of Ile352 of CLR. Given the increase in basal activity it is possible that these residues may help constrain an inactive receptor conformation. This effect may be mediated by intra-helical packing within the CLR or *via* RAMP1 interactions. This adds to earlier work showing that TM6 of CLR is needed for CGRP receptor signal transduction [3].

In conclusion, it is clear that both ECL1 and ECL3 of CLR are essential in the normal functioning of the CGRP receptor. Novel molecular determinants have been found that enhance and impair both the affinity and efficacy of the receptor. Within ECL1 and its associated TM regions are key residues that regulate both the binding and the efficacy of αCGRP. ECL3 and its associated TM domains are important for cell surface receptor expression, possibly by promoting RAMP1 association. Furthermore there are also individual residues, which contribute to recognition of αCGRP and its efficacy. It remains to be shown whether residues within the loops are in direct contact with αCGRP. This study will aid further efforts to probe the extracellular surface of the CGRP receptor along with RAMP1/CLR interface and guide future experiments to map out the large diffuse pharmacophore of αCGRP.

Acknowledgements

We would like to thank Prof. Christopher Reynolds and his group for sharing their progress in the development of their alignment strategy. This work was funded by a studentship awarded to James Barwell by the British Heart Foundation (FS/05/054).

Appendix A. Supplementary data

Supplementary data to this article can be found online at doi:10.1016/j.bbamcr.2011.06.005.

References

[1] J. Barwell, P.S. Miller, D. Donnelly, D.R. Poyner, Mapping interaction sites within the N-terminus of the calcitonin gene-related peptide receptor; the role of residues 23–60 of the calcitonin receptor-like receptor, Peptides 31 (2010) 170–176.
[2] C. Bergwitz, S.A. Jusseaume, M.D. Luck, H. Juppner, T.J. Gardella, Residues in the membrane-spanning and extracellular loop regions of the parathyroid hormone (PTH)-2 receptor determine signaling selectivity for PTH and PTH-related peptide, J. Biol. Chem. 272 (1997) 28861–28868.
[3] A.C. Conner, D.L. Hay, J. Simms, S.G. Howitt, M. Schindler, D.M. Smith, et al., A key role for transmembrane prolines in calcitonin receptor-like receptor agonist binding and signalling: implications for family B G-protein-coupled receptors, Mol. Pharmacol. 67 (2005) 20–31.
[4] A.C. Conner, J. Simms, S.G. Howitt, M. Wheatley, D.R. Poyner, Multiple residues within the second extracellular loop of the CL receptor are required for receptor activation by CGRP pA2 Online, Vol. 3, 2005, p. 99.
[5] M. Conner, M.R. Hicks, T. Dafforn, T.J. Knowles, C. Ludwig, S. Staddon, et al., Functional and biophysical analysis of the C-terminus of the CGRP-receptor; a family B GPCR, Biochemistry 47 (2008) 8434–8444.
[6] E. Di Paolo, J.P. Vilardaga, H. Petry, N. Moguilevsky, A. Bollen, P. Robberecht, et al., Role of charged amino acids conserved in the vasoactive intestinal polypeptide/secretin family of receptors on the secretin receptor functionality, Peptides 20 (1999) 1187–1193.
[7] T.J. Dolinsky, P. Czodrowski, H. Li, J.E. Nielsen, J.H. Jensen, G. Klebe, et al., PDB2PQR: expanding and upgrading automated preparation of biomolecular structures for molecular simulations, Nucleic Acids Res. 35 (2007) W522–W525.
[8] M. Dong, R.F. Cox, L.J. Miller, Juxtamembranous region of the amino terminus of the family B G protein-coupled calcitonin receptor plays a critical role in small-molecule agonist action, J. Biol. Chem. 284 (2009) 21839–21847.
[9] M. Dong, P.C. Lam, D.I. Pinon, A. Orry, P.M. Sexton, R. Abagyan, et al., Secretin occupies a single protomer of the homodimeric secretin receptor complex: insights from photoaffinity labeling studies using dual sites of covalent attachment, J. Biol. Chem. 285 (2010) 9919–9931.
[10] K. Du, P. Nicole, A. Couvineau, M. Laburthe, Aspartate 196 in the first extracellular loop of the human VIP1 receptor is essential for VIP binding and VIP-stimulated cAMP production, Biochem. Biophys. Res. Commun. 230 (1997) 289–292.
[11] K.G. Harikumar, J. Simms, G. Christopoulos, P.M. Sexton, L.J. Miller, Molecular basis of association of receptor activity-modifying protein 3 with the family B G protein-coupled secretin receptor, Biochemistry 48 (2009) 11773–11785.
[12] S. Hilairet, C. Belanger, J. Bertrand, A. Laperriere, S.M. Foord, M. Bouvier, Agonist-promoted internalization of a ternary complex between calcitonin receptor-like receptor, receptor activity-modifying protein 1 (RAMP1), and beta-arrestin, J. Biol. Chem. 276 (2001) 42182–42190.
[13] M.H. Holtmann, S. Ganguli, E.M. Hadac, V. Dolu, L.J. Miller, Multiple extracellular loop domains contribute critical determinants for agonist binding and activation of the secretin receptor, J. Biol. Chem. 271 (1996) 14944–14949.
[14] W. Im, M. Feig, C.L. Brooks 111, An implicit membrane generalized born theory for the study of structure, stability, and interactions of membrane proteins, Biophys. J. 85 (2003) 2900–2918.
[15] I. Langer, P. Vertongen, J. Perret, M. Waelbroeck, P. Robberecht, Lysine 195 and aspartate 196 in the first extracellular loop of the VPAC1 receptor are essential for high affinity binding of agonists but not of antagonists, Neuropharmacology 44 (2003) 125–131.
[16] R.A. Laskowski, PDBsum: summaries and analyses of PDB structures, Nucleic Acids Res. 29 (2001) 221–222.
[17] R.A. Laskowski, D.S. Moss, J.M. Thornton, Main-chain bond lengths and bond angles in protein structures, J. Mol. Biol. 231 (1993) 1049–1067.
[18] H. Li, A.D. Robertson, J.H. Jensen, Very fast empirical prediction and rationalization of protein pKa values, Proteins 61 (2005) 704–721.
[19] L.M. McLatchie, N.J. Fraser, M.J. Main, A. Wise, J. Brown, N. Thompson, et al., RAMPs regulate the transport and ligand specificity of the calcitonin-receptor-like receptor, Nature 393 (1998) 333–339.
[20] L.J. Miller, Q. Chen, P.C. Lam, D.I. Pinon, P.M. Sexton, R. Abagyan, et al., Refinement of glucagon-like peptide 1 docking to its intact receptor using mid-region photolabile probes and molecular modeling, J. Biol. Chem. 286 (2011) 15895–15907.
[21] P. Monaghan, B.E. Thomas, I. Woznica, A. Wittelsberger, D.F. Mierke, M. Rosenblatt, Mapping peptide hormone–receptor interactions using a disulfide-trapping approach, Biochemistry 47 (2008) 5889–5895.
[22] C. Parthier, S. Reedtz-Runge, R. Rudolph, M.T. Stubbs, Passing the baton in class B GPCRs: peptide hormone activation via helix induction? Trends Biochem. Sci. 34 (2009) 303–310.
[23] M.C. Peeters, G.J. van Westen, Q. Li, A.P. Ijzerman, Importance of the extracellular loops in G protein-coupled receptors for ligand recognition and receptor activation, Trends Pharmacol. Sci. 32 (2011) 35–42.
[24] M.M. Rosenkilde, T. Benned-Jensen, T.M. Frimurer, T.W. Schwartz, The minor binding pocket: a major player in 7TM receptor activation, Trends Pharmacol. Sci. 31 (2010) 567–574.
[25] S. Runge, C. Gram, H. Brauner-Osborne, K. Madsen, L.B. Knudsen, B.S. Wulff, Three distinct epitopes on the extracellular face of the glucagon receptor

determine specificity for the glucagon amino terminus, J. Biol. Chem. 278 (2003) 28005–28010.
[26] S.P. Sheikh, J.P. Vilardarga, T.J. Baranski, O. Lichtarge, T. Iiri, E.C. Meng, et al., Similar structures and shared switch mechanisms of the beta2-adrenoceptor and the parathyroid hormone receptor. Zn(II) bridges between helices III and VI block activation, J. Biol. Chem. 274 (1999) 17033–17041.
[27] J. Simms, D.L. Hay, R.J. Bailey, G. Konycheva, G. Bailey, M. Wheatley, et al., Structure–function analysis of RAMP1 by alanine mutagenesis, Biochemistry 48 (2009) 198–205.
[28] C.S. Soto, M. Fasnacht, J. Zhu, L. Forrest, B. Honig, Loop modeling: sampling, filtering, and scoring, Proteins 70 (2008) 834–843.
[29] E. ter Haar, C.M. Koth, N. Abdul-Manan, L. Swenson, J.T. Coll, J.A. Lippke, et al., Crystal structure of the ectodomain complex of the CGRP receptor, a class-B GPCR, reveals the site of drug antagonism, Structure 18 (2010) 1083–1093.
[30] S. Vohra, S.V. Chintapalli, C.J. Illingworth, P.J. Reeves, P.M. Mullineaux, H.S. Clark, et al., Computational studies of family A and family B GPCRs, Biochem. Soc. Trans. 35 (2007) 749–754.
[31] Z. Xiang, C.S. Soto, B. Honig, Evaluating conformational free energies: the colony energy and its application to the problem of loop prediction, Proc. Natl. Acad. Sci. U. S. A. 99 (2002) 7432–7437.
[32] F. Xu, H. Wu, V. Katritch, G.W. Han, K.A. Jacobson, Z.G. Gao, et al., Structure of an agonist-bound human A2A adenosine receptor, Science 332 (2011) 322–327.